Martín-Mateos, P., Khan, F. U. & Bonilla-Manrique, O. E. (2020). Direct hyperspectral dual-comb imaging. Optica, 7(3), 199-202.

DOI: 10.1364/optica.382887

Letter

optica

Direct hyperspectral dual-comb imaging

PEDRO MARTÍN-MATEOS,[1,*] FARID ULLAH KHAN,[1] AND OSCAR ELÍAS BONILLA-MANRIQUE [1]

[1] *Electronics Technology Department, Universidad Carlos III de Madrid, C/Butarque 15, 28911 Leganés, Madrid, Spain*
**Corresponding author: pedro.martin@uc3m.es*

Received XX Month XXXX; revised XX Month, XXXX; accepted XX Month XXXX; posted XX Month XXXX (Doc. ID XXXXX); published XX Month XXXX

Even though dual-comb-based systems are employed almost routinely nowadays in an ever-increasing number of applications, an efficient combination of this effective technique with an imaging arrangement, which would undoubtedly revolutionize hyperspectral imaging, had not yet been demonstrated. Here we present the first hyperspectral dual-comb imaging system in which interferograms are directly detected by a video camera. The system, based on a dual-comb scheme capable of consistently generating interferograms at a rate of 1 Hz and below, combines fast hyperspectral imaging with unprecedented optical resolution and fully multiplex operation. Various proof-of-principle experiments demonstrating hyperspectral imaging of molecular resonances have proved that the direct hyperspectral dual-comb imaging method presented here is capable of characterizing a scene with super-fine resolution in a narrow optical span within one second.

http://dx.doi.org/10.1364/optica.99.099999

1. INTRODUCTION

After the dramatic upsurge in interest in hyperspectral imaging sparkled by many impressive experimental demonstrations [1–5], the aim of a dual-comb spectro-imager has been pursued by several research groups in recent years. An efficient combination of dual frequency comb spectroscopy [6,7] with an imaging system would revolutionize the performance of current hyperspectral imagers, giving rise to a completely new range of possibilities and applications. Until now, dual-comb-based hyperspectral imaging has been restricted to a mechanical raster scanning arrangement employing a single high-speed photodetector. In such implementations acquisition speeds are strongly constrained by waiting times between single spectral characterizations. Nonetheless, and besides important fundamental limitations (mainly associated to the acquisition times of the hypercube), extraordinary results have been presented [2,5]. More recently, and in an attempt to avoid the use of mechanical moving components, a single-pixel detector combined with Hadamard structured illumination (generated by a liquid-crystal-on-silicon spatial light modulator) has enabled the first scan-less dual-comb imaging scheme [8]. However, the increase in acquisition speed provided by the method has so far been limited. In this paper we report, to the best of our knowledge, the first direct hyperspectral dual-comb imaging (DHDCI) architecture in which interferograms are directly acquired by a camera. The method uses a near-infrared free-running dual electro-optic frequency comb system generating interferograms at rates of 0.5 to 1 Hz that can be detected by a regular InGaAs camera. In the first experimental demonstration, and in clear contrast with previous results, we prove that an accurate dual-comb spectral and spatial characterization of a sample can be performed by all the pixel of a camera simultaneously within a single second enabling dynamic video-rate hyperspectral analysis.

2. METHODS

Electro-optic comb generators [9–16] have proved important advantages over conventional mode-locked laser-based architectures, as are tailored spectral coverage and optical resolution [17], frequency agility [11], exquisite simplicity and high acquisition rates [18]. The method presented exploits, above all, the inherently high mutual coherence between combs that enables mHz intermode beat note linewidths [19,20] and virtually unmatched spectral compression ratios. Indeed, in the experiments presented in this paper, spectral compression ratios in excess of 10^{10} have been employed to squeeze the multiheterodyne RF beat note spectrum within 10 Hz. In consequence, very low frequency interferograms can be generated, enabling multiheterodyne detection by a camera operating at regular video rates.

The design of the dual-comb system employed, as sketched in Fig. 1(a), is based on an all-fiber electro-optic architecture: a monochromatic optical seed is injected into two separate acousto-optic modulators that are followed by two electro-optic phase modulators. In this manner, the optical input can be wavelength-shifted by two marginally different frequencies to originate slightly detuned signals from which the two combs can be generated by non-linear phase (or intensity) modulation. After recombination, the dual-comb signal is used to illuminate the scene and the camera sensor captures the diffusely reflected light. The individual pixel-by-pixel Fourier transformation of the temporal evolution of intensity detected by each spatial element yields the final spectral hypercube. Figure 1(b) depicts an actual DHDCI interferogram (digitized in this case at high frequency) of a 9 teeth comb and its Fourier transformation for an offset frequency between combs of 6 Hz and a difference in repetition rates of 1 Hz.

Our DHDCI system has been implemented using a wavelength selected 1531.5 nm diode laser module (QPhotonics) that is driven at

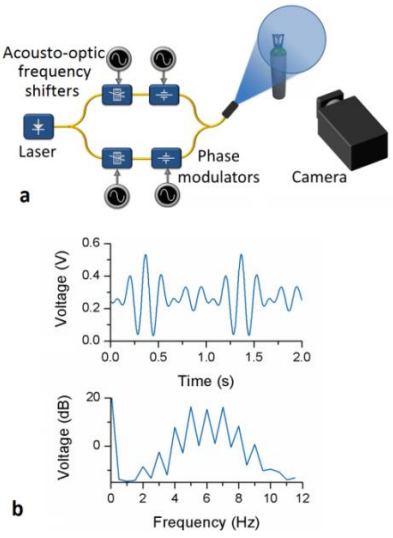

Fig. 1. Fundamentals of direct hyperspectral dual-comb imaging. (a) Block diagram of the electro-optic dual-comb imaging system. (b) Interference between the closely matched combs generates extraordinarily slow interferograms that can be detected by a regular camera. After the Fourier transformation of this signal the optical teeth intensities are retrieved.

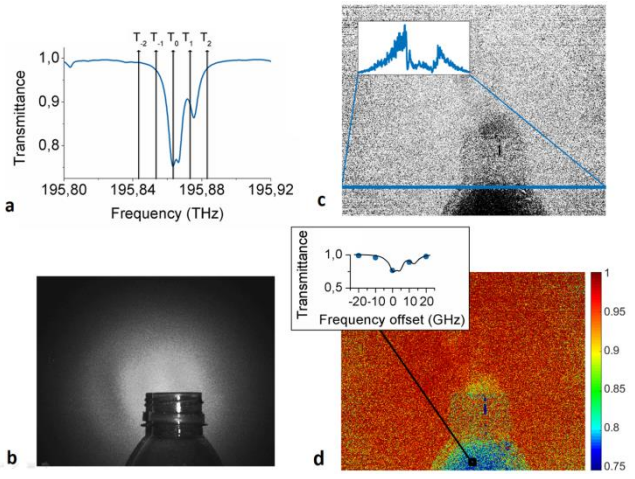

Fig. 2. Experimental demonstration of direct hyperspectral dual-comb imaging of ammonia. (a) Targeted ammonia transition (HITRAN simulation) with a superimposed frequency comb that represents the configuration employed in the experiments. (b) Photograph of the scene during dual-comb illumination (c) Ratio of the intensities retrieved for the comb teeth at T_0 and at T_{-1}. The inset shows the average intensity level at a particular horizontal line of the scene. (d) Map of ammonia transmittance extracted from a single interferogram (327,680 individual spatial elements are interrogated in single second); the inset shows an example of the spectral response detected by the system for a particular pixel (together with a HITRAN simulation) with respect to the offset frequency from 6528.77 cm^{-1}.

80 mA and 26 °C by a low noise current and thermal control unit. The laser emits 14 mW of optical power at a central wavelength of 1531.68 nm (6528.77 cm^{-1}). The signal from the laser is split in two by a filter coupler and taken to the two 40 MHz acousto-optic modulators (Gooch and Housego) operating as frequency shifters. Whereas one of the modulators is driven at 40 MHz, the second is operated at 40 MHz + 6 Hz. The two driving signals are generated by a phase coherent multi-channel synthesizer (Holzworth Instrumentation). Ultra-low-V_π (3 V at 1GHz), 10 GHz lithium niobate phase modulators with external RF termination (EOSPACE) were used to generate the two optical frequency combs. In the experimental demonstrations presented in this paper the phase modulators were firstly driven at f_{rep11} = 10 GHz and $f_{rep12} = f_{rep11}$ + 1 Hz for an optical resolution of 10 GHz and a difference in repetition frequencies Δf_{rep1} = 1 Hz. This configuration is employed to target the spectral feature with a small number of teeth in order maximize the signal-to-noise ratio of the measurement. On a second experimental configuration, aiming at demonstrating ultra-fine optical resolution, the repetition frequencies of the combs were decreased to f_{rep21} = 1 GHz and $f_{rep22} = f_{rep21}$ + 0.5 Hz. A 20 GHz two-channel low phase-noise synthesizer (AnaPico), synchronized to the rest of signal generators in the system, provides these two additional signals. The RF power inputted to the modulators is adjusted as required to generate combs with different numbers of teeth. A second 50/50 splitter recombines the two combs; the output fiber is finally connected to a terminated fiber adapter to illuminate the scene with a remaining average power of roughly 200 μW (due to the insertion losses of modulators and couplers). Only polarization maintaining components and fibers and FC/APC connectors were employed.

An InGaAs camera (C12741-03, Hamamatsu), with a spatial resolution of 640 × 512 pixels, is employed to capture the diffusely reflected light intensity at a frequency of 24 frames per second (synchronized with the rest of signal generators in the system). Images are saved as independent TIFF files. A Matlab script was written to open the complete set of images and, for each pixel: (1) extract the time-changing intensity (interferogram), (2) perform the Fourier transformation, (3) select the frequencies of interest, (4) save all the data and present the results.

3. RESULTS AND DISCUSSION

To validate the performance of the DHDCI scheme, a proof-of-principle experiment demonstrating hyperspectral imaging of molecular resonances has been performed. Specifically, and as represented in Fig. 2 (a) the combination band $\nu_1 + \nu_3$ and the overtone $2\nu_3$ of ammonia at 6529 cm^{-1} is targeted by a tailored five teeth dual-comb illumination signal (with f_{rep11} = 10 GHz and Δf_{rep1} = 1 Hz). The sample, see Fig. 2 (b), is placed within the measurement area, of 100 × 120 mm^2 (for a spatial resolution of 200 × 200 μm^2), situated 60 cm away from the fiber adapter and the camera. 50 mL of a 4% solution of ammonia in water are poured into a PET bottle 10 seconds before targeting gas-phase ammonia in the head-space above the liquid reservoir (most of the light collected by the camera sensor has been diffusely back reflected from the laboratory wall behind the camera).

Some of the first results of the tests are shown in Fig. 2 (c), in which the intensity ratio between the comb teeth at 6528.77 cm^{-1}, T_0 in Fig. 2 (a), and at 6528.44 cm^{-1} (T_{-1}) is plotted (a ratio permits a straightforward compensation of the non-uniform illumination of the scene, as a reference the average intensity for a horizontal line is shown in the inset of Fig. 2 (c)). Whereas the T_0 tooth was precisely tuned to the central frequency of the main absorption feature, the latter (T_{-1}, 10 GHz away) is barely absorbed by the wing of the molecular transition (the teeth frequencies were precalibrated using a low pressure ammonia gas cell). Remarkably, in this experiment all the spectral elements are simultaneously retrieved for the 327,680 pixels of the camera sensor from a single unaveraged and unapodized interferogram in a single second (the interferogram, with a rate of 1 Hz, was acquired at 24 frames per second; spectral information was

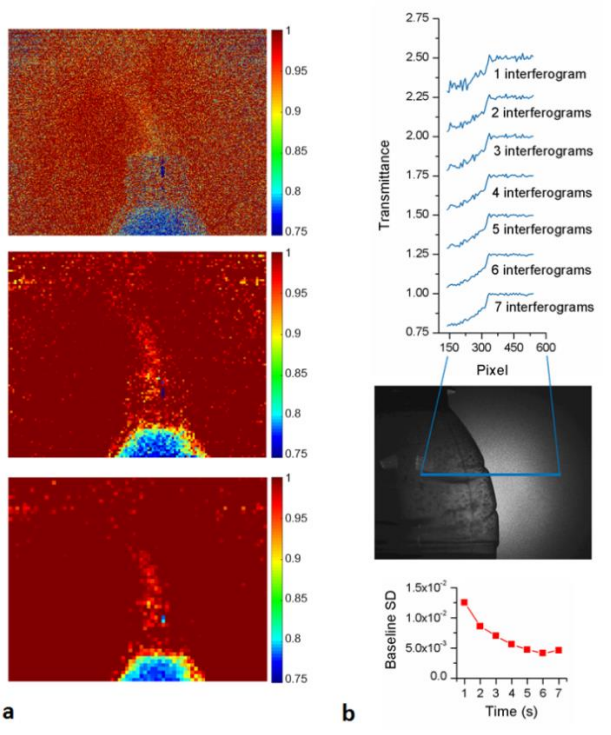

Fig. 3. Averaging procedures for enhancing the signal-to-noise ratio. (a) Map of spectral transmittance directly calculated from a hypercube retrieved from a single interferogram. The raw (upper) results and the 5 by 5 (middle) and 9 by 9 (bottom) pixels averaging maps are compared. (b) Ammonia transmittance retrieved for a single horizontal line of the scene, highlighted by the blue line in the picture, is calculated for an increasing number of interferograms. The noise level is shown in the inset located at the bottom part of the figure.

obtained by the Fourier transformation of the 24 samples and no post-processing was employed). The spectral transmittance calculated for the targeted transition (after normalizing the ratio of Fig. 2 (c) by the difference in intensity in the selected comb lines in the illumination signal) is shown in Fig. 2(d). The inset in Fig. 2 (d) displays the spectral measurement provided by the system (blue dots) in a particular pixel together with a HITRAN fit (black line). The results demonstrate for the first time direct ultra-fine dual-comb imaging performed by a regular camera. Besides this, the one-second time scale enables a completely new level of performance in comparison with previous approaches allowing for dynamic hyperspectral imaging (see Visualization 1, raw interferogram, and Visualization 2, the resulting spectral transmittance calculated with 3 by 3 pixel averaging).

Several averaging procedures, spatial and/or temporal, can certainly be applied to enhance the signal-to-noise ratio of the spectral hypercube. Figure 3 (a) shows a comparison between a raw calculation of transmittance and the 5 by 5 and 9 by 9 pixel averaging images (unweighted averages). As before, a single interferogram was processed to obtain the bidimensional map of transmittance. This direct comparison demonstrates that a 9 by 9 pixel averaging is sufficient to provide an utterly clear picture of the absorption of the targeted molecular resonance for a final resolution of 4000 pixels (it is worthwhile noting again that the hypercube was retrieved from 24 frames acquired in one second). In this particular example, the only noisy spots at the top of the image coincide with areas in which the illumination intensity was very limited.

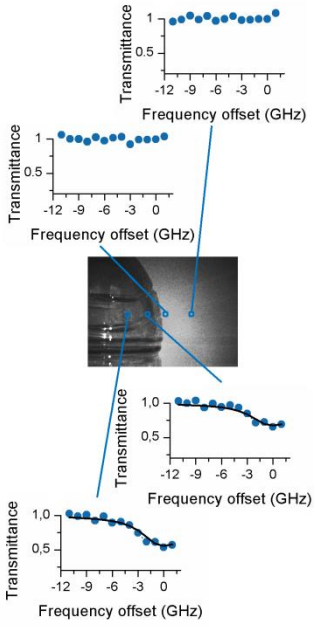

Fig. 4. Ultra-high resolution direct hyperspectral dual-comb imaging. The abscissa axis represents the frequency detuning from the 6528.77 cm^{-1} comb tooth.

Similarly, on a static sample time-averaging can be employed to increase the spectroscopic signal-to-noise ratio. For this experiment gas ammonia in the head-space of the bottle is targeted 60 second after pouring the solution of liquid NH_3 and sealing the bottle. As shown in Fig. 3(b), the absorbance-depth profile is calculated for a horizontal line of the sample (highlighted in blue in the picture) for an increasing number of interferograms. The evolution of the standard deviation of the baseline is shown in the inset at the bottom of the figure. Even though time-averaging enhances the performance following a quasi-ideal trend, in this experimental demonstration the maximum integration time of the system is limited to roughly 6 seconds by interferometric phase noise within the dual-comb arrangement (that has not been stabilized neither in phase nor in temperature). This effect limits the noise level to 4.5×10^{-3} (calculated as the standard deviation of the baseline, pixels from position 350 to 600) for a 1σ limit of detection of around 150 ppm×m. To this respect, simple phase stabilization/compensation mechanisms [19–22] can be employed to straightforwardly expand the coherence time of the dual-comb source.

In a final demonstration, fast ultra-high resolution hyperspectral imaging has been demonstrated by accurately characterizing the absorption line shape under test using a dual-comb configuration with thirteen teeth and 1 GHz (repetition frequencies of f_{rep21} = 1 GHz and Δf_{rep2} = 0.5 Hz) optical spacing (resolution). The interferogram period was expanded to two seconds to account for the larger number of teeth, whereas the frame rate of the camera was maintained at 24 frames per second. The spectral response of the target, characterized at four particular spatial locations, is shown in Fig. 4 for a single interferogram acquisition and 5 by 5 pixel averaging. As shown in the two upper spectra, areas without a selective absorber yield a flat transmittance profile regardless of the illumination intensity. However, an accurate line shape characterization of the lower frequency half of the molecular transition is retrieved from the points of the scene in which ammonia is present. The accuracy of the results is confirmed by the simulation using the HITRAN database, superimposed in black,

providing R^2 values of 0.96 and 0.95 respectively with root mean square errors of roughly 3%. Concentrations of 26380 and 16600 ppm×m are retrieved from the fitting. During this spectro-imaging characterization, performed in 2 seconds, an optical span of 12 GHz is analyzed by the 327,680 pixels of camera simultaneously for a total number of 4.25 million spectral elements acquired.

4. CONCLUDING REMARKS

In conclusion, electro-optic dual-comb generators provide a flawless combination of resolution, accuracy and flexibility that enables the generation of tailored combs capable of providing the basis for from a narrow ultra-accurate high-resolution spectral characterization to an octave spanning comb coverage for the electronic synthesis of light [11,13,23,24]. The method presented in this manuscript now offers the possibility of taking full advantage of these features for the implementation of a direct hyperspectral imaging set-up. To this respect, we have proved that a properly designed dual-comb optical source is capable of transforming a regular video camera into an ultra-high resolution hyperspectral dual-comb imager to provide a combination of both spectral and spatial information. This technique provides a fully multiplex approach in which the low-frequency interferograms are detected by all the pixels of the camera synchronously to provide simultaneous spectral and spatial characterization. Noticeably, the utterly simple dual-comb arrangement employed, operating in free running and without any stabilization or compensation mechanisms (very well suited for field deployment), has enabled complete spectro-imaging characterizations for 327,680 pixels simultaneously in a single second, more than three orders of magnitude faster than previous approaches. Several dynamic and static proof-of-principle experiments have demonstrated the potential of our method for the rapid acquisition of targeted hyperspectral dual-comb images for a moderate spectral span. However, the number of detectable teeth is only restricted by the required spectral resolution after Fourier transformation and the camera frame rate, and will easily reach up to thousands of lines in the very near future thanks to the growing availability of high-speed cameras [25]. These new systems will not only be able to cover wide spectral spans, but also to operate with high signal-to noise ratios at acquisition rates that could exceed 100 hypercubes per second. These numbers can nonetheless be strikingly scaled up if sub-window mode (smaller frame size) is employed in the acquisition, and certainly with future advances in technology. Beyond intensity spectral characterization, DHDCI also enables phase imaging with a dispersive dual-comb interferometric scheme, which could transform not only chemical mapping or label-free biomedical sensing, but also high-accuracy 3D mapping. Besides this, a near-infrared electro-optic comb can be straightforwardly shifted to mid-IR frequencies [26,27], to markedly enhance the sensitivity of the system, and to the THz range [28] (where off-the-shelf cameras of up to 0.1 megapixels are already available), to provide a much wider relative span and the strong possibility to revolutionize nondestructive testing and product inspection in food, agricultural and pharmaceutical industries.

Funding. This project has received funding from the ATTRACT project funded by the EC under Grant Agreement 777222.

Acknowledgment. We thank V. Sánchez and D. Castrillo (Hamamatsu) for the loan of the NIR camera.

Disclosures. The authors declare no conflicts of interest

See Supplement 1 for supporting content.

REFERENCES

1. D. Bannon, Nat. Photonics **3**,627 (2009).
2. T. Ideguchi, S. Holzner, B. Bernhardt, G. Guelachvili, N. Picqué, and T. W. Hänsch, Nature **502**, 355 (2013).
3. X. Hadoux, F. Hui, J. K. H. Lim, C. L. Masters, A. Pébay, S. Chevalier, J. Ha, S. Loi, C. J. Fowler, C. Rowe, V. L. Villemagne, E. N. Taylor, C. Fluke, J.-P. Soucy, F. Lesage, J.-P. Sylvestre, P. Rosa-Neto, S. Mathotaarachchi, S. Gauthier, Z. S. Nasreddine, J. D. Arbour, M.-A. Rhéaume, S. Beaulieu, M. Dirani, C. T. O. Nguyen, B. V. Bui, R. Williamson, J. G. Crowston, and P. van Wijngaarden, Nat. Commun. **10**, 4227 (2019).
4. I. Amenabar, S. Poly, M. Goikoetxea, W. Nuansing, P. Lasch, and R. Hillenbrand, Nat. Commun. **8**, 14402 (2017).
5. L. A. Sterczewski, J. Westberg, Y. Yang, D. Burghoff, J. Reno, Q. Hu, and G. Wysocki, Optica **6**, 766 (2019).
6. I. Coddington, N. Newbury, and W. Swann, Optica **3**, 414 (2016).
7. N. Picqué and T. W. Hänsch, Nat. Photonics **13**, 146 (2019).
8. K. Shibuya, T. Minamikawa, Y. Mizutani, H. Yamamoto, K. Minoshima, T. Yasui, and T. Iwata, Opt. Express **25**, 21947 (2017).
9. D. A. Long, A. J. Fleisher, K. O. Douglass, S. E. Maxwell, K. Bielska, J. T. Hodges, and D. F. Plusquellic, Opt. Lett. **39**, 2688 (2014).
10. P. Martin-Mateos, M. Ruiz-Llata, J. Posada-Roman, and P. Acedo, IEEE Photonics Technol. Lett. **27**, 1309 (2015).
11. G. Millot, S. Pitois, M. Yan, T. Hovannysyan, A. Bendahmane, T. W. Hänsch, and N. Picqué, Nat. Photonics **10**, 27 (2016).
12. P. Martín-Mateos, B. Jerez, and P. Acedo, Opt. Express **23**, 21149 (2015).
13. D. R. Carlson, D. D. Hickstein, W. Zhang, A. J. Metcalf, F. Quinlan, S. A. Diddams, and S. B. Papp, Science **361**, 1358 (2018).
14. A. J. Metcalf, C. D. Fredrick, R. C. Terrien, S. B. Papp, S. A. Diddams, Opt. Lett. **44**, 2673 (2019).
15. S. T. Cundiff and A. M. Weiner, Nat. Photonics **4**, 760 (2010).
16. A. J. Metcalf, T. Anderson, C. F. Bender, S. Blakeslee, W. Brand, D. R. Carlson, W. D. Cochran, S. A. Diddams, M. Endl, C. Fredrick, S. Halverson, D. D. Hickstein, F. Hearty, J. Jennings, S. Kanodia, K. F. Kaplan, E. Levi, E. Lubar, S. Mahadevan, A. Monson, J. P. Ninan, C. Nitroy, S. Osterman, S. B. Papp, F. Quinlan, L. Ramsey, P. Robertson, A. Roy, C. Schwab, S. Sigurdsson, K. Srinivasan, G. Stefansson, D. A. Sterner, R. Terrien, A. Wolszczan, J. T. Wright, and G. Ycas, Optica **6**, 233 (2019).
17. K. Fdil, V. Michaud-Belleau, N. B. Hébert, P. Guay, A. J. Fleisher, J.-D. Deschênes, and J. Genest, Opt. Lett. **44**, 4415 (2019).
18. V. Durán, S. Tainta, and V. Torres-Company, Opt. Express **23**, 30557 (2015).
19. A. J. Fleisher, D. A. Long, Z. D. Reed, J. T. Hodges, and D. F. Plusquellic, Opt. Express **24**, 10424 (2016).
20. P. Martín-Mateos, B. Jerez, P. Largo-Izquierdo, and P. Acedo, Opt. Express **26**, 9700 (2018).
21. J. Roy, J.-D. Deschênes, S. Potvin, and J. Genest, Opt. Express **20**, 21932 (2012).
22. L. A. Sterczewski, J. Westberg, G. Wysocki, J. Westberg, and G. Wysocki, Opt. Express **27**, 23875 (2019).
23. K. Beha, D. C. Cole, P. Del'Haye, A. Coillet, S. A. Diddams, and S. B. Papp, Optica **4**, 406 (2017).
24. P. Guay, J. Genest, and A. J. Fleisher, Opt. Lett. **43**, 1407 (2018).
25. J. Neys, J. Bentell, M. O'Grady, J. Vermeiren, T. Colin, P. Hooylaerts, and B. Grietens, in SPIE Remote Sensing 2008, **7106**, 71061M (International Society for Optics and Photonics).
26. E. Baumann, F. R. Giorgetta, W. C. Swann, A. M. Zolot, I. Coddington, and N. R. Newbury, Phys. Rev. A **84**, 062513 (2011).
27. M. Yan, P.-L. Luo, K. Iwakuni, G. Millot, T. W. Hänsch, and N. Picqué, Light Sci. Appl. **6**, e17076 (2017).
28. B. Jerez, F. Walla, A. Betancur, P. Martín-Mateos, C. de Dios, and P. Acedo, Opt. Lett. **44**, 415 (2019).

FULL REFERENCES

1. D. Bannon, "Cubes and slices," Nat. Photonics 3(11), 627–629 (2009).
2. T. Ideguchi, S. Holzner, B. Bernhardt, G. Guelachvili, N. Picqué, and T. W. Hänsch, "Coherent Raman spectro-imaging with laser frequency combs," Nature 502(7471), 355–358 (2013).
3. X. Hadoux, F. Hui, J. K. H. Lim, C. L. Masters, A. Pébay, S. Chevalier, J. Ha, S. Loi, C. J. Fowler, C. Rowe, V. L. Villemagne, E. N. Taylor, C. Fluke, J.-P. Soucy, F. Lesage, J.-P. Sylvestre, P. Rosa-Neto, S. Mathotaarachchi, S. Gauthier, Z. S. Nasreddine, J. D. Arbour, M.-A. Rhéaume, S. Beaulieu, M. Dirani, C. T. O. Nguyen, B. V. Bui, R. Williamson, J. G. Crowston, and P. van Wijngaarden, "Non-invasive in vivo hyperspectral imaging of the retina for potential biomarker use in Alzheimer's disease," Nat. Commun. 10(1), 4227 (2019).
4. I. Amenabar, S. Poly, M. Goikoetxea, W. Nuansing, P. Lasch, and R. Hillenbrand, "Hyperspectral infrared nanoimaging of organic samples based on Fourier transform infrared nanospectroscopy," Nat. Commun. 8(1), 14402 (2017).
5. L. A. Sterczewski, J. Westberg, Y. Yang, D. Burghoff, J. Reno, Q. Hu, and G. Wysocki, "Terahertz hyperspectral imaging with dual chip-scale combs," Optica 6(6), 766 (2019).
6. I. Coddington, N. Newbury, and W. Swann, "Dual-comb spectroscopy," Optica 3(4), 414–426 (2016).
7. N. Picqué and T. W. Hänsch, "Frequency comb spectroscopy," Nat. Photonics 13(3), 146–157 (2019).
8. K. Shibuya, T. Minamikawa, Y. Mizutani, H. Yamamoto, K. Minoshima, T. Yasui, and T. Iwata, "Scan-less hyperspectral dual-comb single-pixel-imaging in both amplitude and phase," Opt. Express 25(18), 21947 (2017).
9. D. A. Long, A. J. Fleisher, K. O. Douglass, S. E. Maxwell, K. Bielska, J. T. Hodges, and D. F. Plusquellic, "Multiheterodyne spectroscopy with optical frequency combs generated from a continuous-wave laser.," Opt. Lett. 39(9), 2688–2690 (2014).
10. P. Martin-Mateos, M. Ruiz-Llata, J. Posada-Roman, and P. Acedo, "Dual-comb architecture for fast spectroscopic measurements and spectral characterization," IEEE Photonics Technol. Lett. 27(12), 1309–1312 (2015).
11. G. Millot, S. Pitois, M. Yan, T. Hovannysyan, A. Bendahmane, T. W. Hänsch, and N. Picqué, "Frequency-agile dual-comb spectroscopy," Nat. Photonics 10, 27–30 (2016).
12. P. Martín-Mateos, B. Jerez, and P. Acedo, "Dual electro-optic optical frequency combs for multiheterodyne molecular dispersion spectroscopy," Opt. Express 23(16), 21149–21158 (2015).
13. D. R. Carlson, D. D. Hickstein, W. Zhang, A. J. Metcalf, F. Quinlan, S. A. Diddams, and S. B. Papp, "Ultrafast electro-optic light with subcycle control.," Science 361(6409), 1358–1363 (2018).
14. A. J. Metcalf, C. D. Fredrick, R. C. Terrien, S. B. Papp, S. A. Diddams, , "30 GHz electro-optic frequency comb spanning 300 THz in the near infrared and visible," Opt. Lett. 44(11), 2673 (2019).
15. S. T. Cundiff and A. M. Weiner, "Optical arbitrary waveform generation," Nat. Photonics 4(11), 760–766 (2010).
16. A. J. Metcalf, T. Anderson, C. F. Bender, S. Blakeslee, W. Brand, D. R. Carlson, W. D. Cochran, S. A. Diddams, M. Endl, C. Fredrick, S. Halverson, D. D. Hickstein, F. Hearty, J. Jennings, S. Kanodia, K. F. Kaplan, E. Levi, E. Lubar, S. Mahadevan, A. Monson, J. P. Ninan, C. Nitroy, S. Osterman, S. B. Papp, F. Quinlan, L. Ramsey, P. Robertson, A. Roy, C. Schwab, S. Sigurdsson, K. Srinivasan, G. Stefansson, D. A. Sterner, R. Terrien, A. Wolszczan, J. T. Wright, and G. Ycas, "Stellar spectroscopy in the near-infrared with a laser frequency comb," Optica 6(2), 233 (2019).
17. K. Fdil, V. Michaud-Belleau, N. B. Hébert, P. Guay, A. J. Fleisher, J.-D. Deschênes, and J. Genest, "Dual electro-optic frequency comb spectroscopy using pseudo-random modulation," Opt. Lett. 44(17), 4415 (2019).
18. V. Durán, S. Tainta, and V. Torres-Company, "Ultrafast electrooptic dual-comb interferometry," Opt. Express 23(23), 30557–30569 (2015).
19. A. J. Fleisher, D. A. Long, Z. D. Reed, J. T. Hodges, and D. F. Plusquellic, "Coherent cavity-enhanced dual-comb spectroscopy," Opt. Express 24(10), 10424–10434 (2016).
20. P. Martín-Mateos, B. Jerez, P. Largo-Izquierdo, and P. Acedo, "Frequency accurate coherent electro-optic dual-comb spectroscopy in real-time," Opt. Express 26(8), 9700 (2018).
21. J. Roy, J.-D. Deschênes, S. Potvin, and J. Genest, "Continuous real-time correction and averaging for frequency comb interferometry," Opt. Express 20(20), 21932–21939 (2012).
22. L. A. Sterczewski, J. Westberg, G. Wysocki, J. Westberg, and G. Wysocki, "Computational coherent averaging for free-running dual-comb spectroscopy," Opt. Express 27(17), 23875 (2019).
23. K. Beha, D. C. Cole, P. Del'Haye, A. Coillet, S. A. Diddams, and S. B. Papp, "Electronic synthesis of light," Optica 4(4), 406–411 (2017).
24. P. Guay, J. Genest, and A. J. Fleisher, "Precision spectroscopy of H 13 CN using a free-running, all-fiber dual electro-optic frequency comb system," Opt. Lett. 43(6), 1407 (2018).
25. J. Neys, J. Bentell, M. O'Grady, J. Vermeiren, T. Colin, P. Hooylaerts, and B. Grietens, "Cheetah: A high frame rate, high resolution SWIR image camera," in R. Meynart, S. P. Neeck, H. Shimoda, and S. Habib, eds. (International Society for Optics and Photonics, 2008), 7106, p. 71061M.
26. E. Baumann, F. R. Giorgetta, W. C. Swann, A. M. Zolot, I. Coddington, and N. R. Newbury, "Spectroscopy of the methane v3 band with an accurate midinfrared coherent dual-comb spectrometer," Phys. Rev. A 84(6), 062513 (2011).
27. M. Yan, P.-L. Luo, K. Iwakuni, G. Millot, T. W. Hänsch, and N. Picqué, "Mid-infrared dual-comb spectroscopy with electro-optic modulators," Light Sci. Appl. 6(10), e17076–e17076 (2017).
28. B. Jerez, F. Walla, A. Betancur, P. Martín-Mateos, C. de Dios, and P. Acedo, "Electro-optic THz dual-comb architecture for high-resolution, absolute spectroscopy," Opt. Lett. 44(2), 415 (2019).